

Planar micro-optic solar concentrator

Jason H. Karp*, Eric J. Tremblay and Joseph E. Ford

Department of Electrical and Computer Engineering, University of California, San Diego
9500 Gilman Drive, La Jolla, CA 92093-0407, USA

*jkarp@ucsd.edu

Abstract: We present a new approach to solar concentration where sunlight collected by each lens in a two-dimensional lens array is coupled into a shared, planar waveguide using localized features placed at each lens focus. This geometry yields a thin, flat profile for moderate concentration systems which may be fabricated by low-cost roll manufacture. We provide analyses of tradeoffs and show optimized designs can achieve 90% and 82% optical efficiency at 73x and 300x concentration, respectively. Finally, we present preliminary experimental results of a concentrator using self-aligned reflective coupling features fabricated by exposing molded SU-8 features through the lens array.

©2010 Optical Society of America

OCIS codes: (350.6050) Solar energy; (220.1770) Concentrators; (230.7400) Waveguides, slab

References and links

1. P. Benitez, and J. C. Minano, "Concentrator optics for the next-generation photovoltaics," in *Next Generation Photovoltaics*, A. Martí and A. Luque, eds. (Institute of Physics, 2004), Ch. 13.
2. R. Winston, J. C. Minano, W. T. Welford, and P. Benitez, *Nonimaging Optics*, (Academic Press 2004).
3. J. M. Gordon, "Concentrator Optics," in *Concentrator Photovoltaics*, A. L. Luque and V. M. Andreev, (Springer, Berlin, 2007), Ch. 6.
4. D. Feuermann, and J. M. Gordon, "High-concentration photovoltaic designs based on miniature parabolic dishes," *Solar Energy*, Vol. **70-5**, 423–430 (2001).
5. R. Winston, and J. M. Gordon, "Planar concentrators near the étendue limit," *Opt. Lett.* **30**(19), 2617–2619 (2005).
6. A. W. Bett, C. Baur, F. Dimroth, G. Lange, M. Meusel, S. Riesen, G. Siefer, V. M. Andreev, V. D. Rumyantsev, and N. A. Sadchikov, "FLATCON™-Modules," *Technology and Characterisation WCPEC-3*, 634–637 (2003).
7. C. Balanis, *Advanced Engineering Electromagnetics*, (John Wiley & Sons, 1989).
8. W. J. Cassarly, "Nonimaging optics: concentration and illumination," in *Handbook of Optics Vol. III*, M. Bass, J. M. Enoch, E. W. Van Stryland and W. L. Wolfe (2nd ed. McGraw-Hill, 1995), Ch. 2.
9. M. H. Chou, M. A. Arbore, and M. M. Fejer, "Adiabatically tapered periodic segmentation of channel waveguides for mode-size transformation and fundamental mode excitation," *Opt. Lett.* **21**(11), 794–796 (1996).
10. M. C. Chien, Y. L. Tung, and C. H. Tien, "Ultracompact backlight-reversed concentration optics," *Appl. Opt.* **48**(21), 4142–4148 (2009).
11. M. P. C. Watts, "Advances in roll to roll processing of optics," *Proc. SPIE* **6883**, 688305 (2008).
12. A. Marcano O, C. Loper, and N. Melikechi, "High-sensitivity absorption measurement in water and glass samples using a mode-mismatched pump-probe thermal lens method," *Appl. Phys. Lett.* **78**(22), 3415 (2001).
13. A. Rabl, *Active solar collectors and their applications*, (Oxford University Press, New York, 1985).
14. J. G. Chang, and Y. B. Fang, "Dot-pattern design of a light guide in an edge-lit backlight using a regional partition approach," *Opt. Eng.* **46**(4), 043002 (2007).
15. W. G. Van Sark, K. W. Barnham, L. H. Slooff, A. J. Chatten, A. Büchtemann, A. Meyer, S. J. Mc.Cormack, R. Koole, D. J. Farrell, R. Bose, E. E. Bende, A. R. Burgers, T. Budel, J. Quilitz, M. Kennedy, T. Meyer, S. H. Wadman, G. P. van Klink, G. van Kotten, A. Meijerink, and D. Vanmaekelbergh, "Luminescent Solar Concentrators - A review of recent results," *Opt. Express* **16**, 21773–21792 (2008).
16. T. Tamir and S. T. Peng, "Analysis and design of grating couplers," *Appl. Phys. A*, **14**, 235–254 (1977).
17. R. K. Kostuk, and G. Rosenberg, "Analysis and design of holographic solar concentrators," *Proc. SPIE* **7043**, 70430I (2008).
18. P. Campbell, and M. A. Green, "Light trapping properties of pyramidally textured surfaces," *J. Appl. Phys.* **62**(1), 243–249 (1987).
19. C. E. Winiarz, "Measurement of light capture in solar cells from silver- and tin-plated patterned bus bars," (S.B. Thesis, Massachusetts Institute of Technology, Dept. of Mech. Eng., 2007).
20. P. J. R. Laybourn, W. A. Gambling and D. T. Jones, "Measurement of attenuation in low-loss optical glass," *Opt. Quantum Electron.* **3**, 137–144 (1971).

21. A. Davis, "Raytrace assisted analytical formulation of Fresnel lens transmission efficiency," *Proc. SPIE* **7429**, 74290D (2009).
 22. G. Khanarian, and H. Celanese, "Optical properties of cyclic olefin copolymers," *Opt. Eng.* **40**(6), 1024–1029 (2001).
 23. A. S. T. M. Standard, G173–03e1, "Standard Tables for Reference Solar Spectral Irradiances: Direct Normal and Hemispherical on 37° Tilted Surface," *Ann. Book of ASTM Standards*, Philadelphia, PA, 2003, DOI: 10.1520/G0173-03E01, www.astm.org.
 24. H. Lorenz, M. Despont, N. Fahrni, N. LaBianca, P. Renaud, and P. Vettiger, "SU-8: a low-cost negative resist for MEMS," *J. Micromech. Microeng.* **7**(3), 121–124 (1997).
 25. R. J. Jackman, T. M. Floyd, R. Ghodssi, M. A. Schmidt, and K. F. Jensen, "Microfluidic systems with on-line UV detection fabricated in photodefinable epoxy," *J. Micromech. Microeng.* **11**(3), 263–269 (2001).
 26. A. T. Cannistra, and T. J. Suleski, "Characterization of hybrid molding and lithography for SU-8 micro-optical components," *Proc. SPIE* **7205**, 720517 (2009).
 27. J. H. Karp, and J. E. Ford, "Planar micro-optic concentration using multiple imaging lenses into a common slab waveguide," *Proc. SPIE* **7407**, 7407–7411 (2009).
-

1. Introduction

Concentrator photovoltaic (CPV) systems use large area optical components to collect direct sunlight and transfer the energy onto small, high-efficiency photovoltaic (PV) cells. CPV systems have the potential for higher overall conversion efficiencies while reducing the quantity of costly, environmentally sensitive semiconductor materials. High concentration systems (>100x) incorporate mechanical tracking to maintain alignment with the sun. System designs should include cell alignment tolerances, angular acceptance, and flux uniformity [1]. For CPV systems to be cost-effective, the complete cost of the optics, assembly and mechanical tracking must not exceed the cost savings gained from using small area PV cells.

High-flux concentrators typically consist of a large primary optic to focus sunlight and a secondary optical element for flux homogenization [2,3]. A common design approach divides the upward-facing primary into several small apertures, each with its own individual secondary element and solar cell. This transforms the overall optical volume into a thin system which can be easily assembled and mounted for two-axis tracking [4–6]. However, integrating hundreds of small PV cells all aligned to their respective optics leads to large-scale connectivity and cost concerns.

In this paper, we investigate an alternative approach for planar concentration by replacing multiple nonimaging secondary optics and their associated PV cells with a single multimode waveguide connected to a shared PV cell. Sunlight collected by each aperture of the arrayed primary is coupled into a common slab waveguide using localized injection features such as prisms, gratings or scattering surfaces. Rays that exceed the critical angle defined by Snell's Law propagate via total internal reflection (TIR) within the waveguide to the exit aperture, typically at the edge of the slab. TIR is a complete reflection with negligible spectral or polarization-dependent losses which enables long propagation lifetimes [7]. Planar waveguides also provide excellent beam homogenization when coupling diverging illumination into a high number of supported modes [8]. The waveguide transports sunlight collected over the entire input aperture to a single PV cell placed at the waveguide edge. PV alignment becomes trivial since comparatively large cells are cemented to the waveguide edge(s). Fewer PV cells reduce connection complexity and allow one heat sink to manage the entire system output. Figure 1 shows the differences between individual secondary optics and a common waveguide secondary.

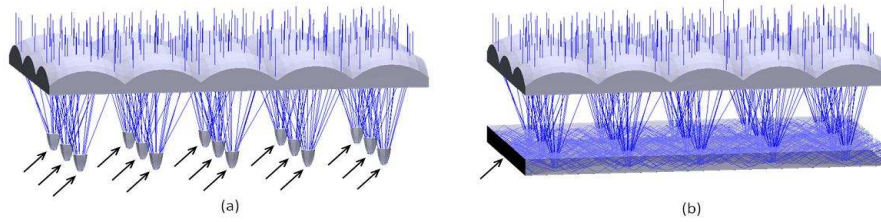


Fig. 1. Individual secondary optics require multiple PV cells (a). A slab waveguide homogenizes and transports sunlight from all apertures to a single cell (b). Increasing the waveguide length does not increase the required PV cell area. Arrows indicate PV cell locations.

Completely efficient waveguide coupling from multiple locations and lossless propagation can only occur through a monotonic increase in modal volume [9]. For example, light guide plates used in flat-panel display backlighting use tapered or stepped-thickness waveguides [10]. Requiring the waveguide thickness to grow as light is collected from each subsequent aperture limits the aspect ratio and therefore the maximum physical length of the concentrator. However, if the system can accept some guiding loss, planar slab waveguides, which maintain the same modal cross-section, can be used. Planar slabs are unlimited in length, but without an increase in modal volume, guided rays can strike a subsequent coupling region and decouple as loss. The number of TIR interactions during propagation to the PV cell affects the likelihood of decoupling and therefore the optical efficiency. Couplers typically cover $<0.1\%$ of the waveguide surface enabling the system to yield both high efficiency and high concentration. Figure 2 highlights the differences between lossless (limited length) and lossy (limited efficiency) waveguiding.

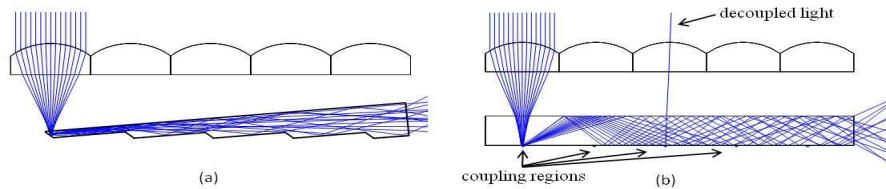


Fig. 2. Coupling without loss requires an increase in modal volume (a). Light within planar waveguides may strike subsequent coupling regions and decouple as loss (b). Coupling regions occupy only a small fraction of the waveguide surface to enable high efficiency.

Our goal was to design a concentrator optic which could be fabricated at an extremely low cost per unit area. Constraining the design to be compatible with a continuous roll-process manufacturing platform, as opposed to injection molded and assembled elements, maximizes the cost advantage of CPV. Roll processing can perform a range of functions on rigid or flexible substrates such as embossing of refractive or diffractive structures, dielectric and metallic deposition and the joining of multiple processed layers [11]. To yield a rapid and continuous flow of integrated optics, the concentrator design must maintain a uniform thickness, thereby limiting our approach to planar waveguides. In this paper, we describe solar concentrators compatible with roll manufacturing by placing a two-dimensional refractive lens array above a planar slab waveguide. We investigate the design tradeoffs as well as present fabrication methods and results for a proof-of-concept prototype. Sections 2 and 3 discuss the concentrator geometry and coupling approaches. We model and optimize the performance of two, high-flux concentrators based on material constraints in Section 4. Section 5 details the fabrication and operation of an initial working prototype, and conclusions are made in Section 6.

2. Concentrator geometry

We define the geometric concentration ratio as the ratio of input to output areas of the optical system. For the planar waveguide concentrator, this ratio is simply the length of the waveguide divided by the thickness, as seen in Eq. (1). In this definition, we assume no concentration along the orthogonal dimension of the waveguide, being the slab width. Optical efficiency η is the fraction of light which reaches the output aperture and principally includes Fresnel reflections, material absorption and waveguide decoupling losses. Equation (2) denotes flux concentration as the product of the geometric concentration ratio and optical efficiency, and indicates the concentration level present at the PV cell. Antireflection coatings minimize surface reflectivity and common optical glass such as BK7 exhibit a very low absorption coefficient ($3 \times 10^{-6} \text{ cm}^{-1}$) at visible wavelengths [12]. Decoupling losses become the primary consideration when defining the concentrator dimensions and performance.

Every lens array aperture forms a demagnified image of the sun which subtends $\pm 0.26^\circ$ [13]. We calculate the aberration-free solar image height using $2f \tan \theta$ where f is the lens focal length and θ is the acceptance half-angle. Each lens element has its own two-dimensional geometric concentration defined by Eq. (3). The lens aperture to image area is expressed in terms of the lens focal length to diameter ratio, or F-number ($F/\#$), and acceptance half-angle. The planar waveguide does not alter the internal ray angles after coupling, and therefore cannot further concentrate guided light based on étendue. In other words, the slab waveguide does not provide concentration in addition to that from each lens, but rather collects, homogenizes and transports the energy to a common exit aperture. When $\theta = 0.26^\circ$, light intensity at the image plane sets an upper bound on flux output levels. Equation (3) is only applicable for imaging lenses and should be modified if using other collection optics such as nonimaging primaries.

$$C_{geo} = \frac{\text{waveguide length}}{\text{waveguide thickness}} \quad (1)$$

$$C_{flux} = \eta \times C_{geo} \quad (2)$$

$$C_{lens} = \frac{1}{(2F/\# \tan \theta)^2} \quad (3)$$

We begin our design by evaluating decoupling losses associated with the concentrator geometry. The inverse of lens concentration C_{lens} yields the fraction of the waveguide surface which contributes to loss during propagation. Lower $F/\#$'s (shorter focal lengths) reduce coupling areas, however, also produce steep marginal rays which may not couple into guided modes of the waveguide. The numerical aperture (NA) of the waveguide defines the maximum supported ray angle. The impact of the waveguide NA on lens $F/\#$ and coupling mechanism is discussed in Section 3.

Consider a light ray which enters a waveguide of length L and thickness H at position P from the exit aperture. After striking the coupler, the ray propagates at an angle ϕ with respect to the bottom surface of the waveguide. The ray traverses a distance $2H/\tan \phi$ along the waveguide until interacting with the back surface, at which point it may undergo TIR or decouple if incident upon a subsequent feature. The total number of surface interactions is inversely proportional to the waveguide thickness and is expressed as $P \tan \phi / 2H$. Figure 3 graphically depicts the described geometry.

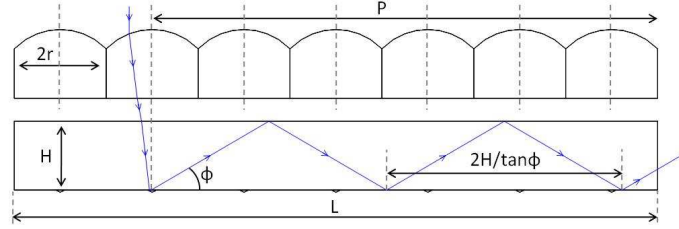


Fig. 3. Graphical representation of the geometry associated with micro-optic concentrator.

Equation (4) calculates the optical efficiency from input position P , expressed as the transmission probability raised to the total number of back surface interactions for each coupled angle ϕ . Equation (5) introduces Fresnel reflection loss R and material absorption by exponential decay of the path length multiplied by the absorption coefficient α . Equation (6) computes the total optical efficiency by considering the efficiency from every lens of diameter $2r$, position P and integrated over all coupled ray angles confined within the waveguide. Figure 4 plots the optical efficiency as functions of slab length and thickness for 2mm diameter, F/3 lenses coupled at $\phi = 60^\circ$ into a BK7 slab surrounded by air. Short, thick waveguides yield the highest efficiency, but offer minimal geometric concentration. Several waveguide configurations provide $>300\times$ geometric concentration with $>90\%$ optical efficiency. However, Fig. 4 only considers rays at one angle within the waveguide. To accurately model optical efficiency, we must consider the entire cone of light at the lens focus as well angles after coupling. In the following section, we discuss various coupling approaches to identify all guided ray angles.

$$\eta_{decouple}(P, \phi) = \left(1 - \frac{1}{C_{lens}}\right)^{\frac{P \tan \phi}{2H}} \quad (4)$$

$$\eta_{position}(P, \phi) = (1 - R) \times \eta_{decouple}(P, \phi) \times \exp(-\alpha P \cos \phi) \quad (5)$$

$$\eta_{total} = \frac{\sum_P \int_{\phi} \eta_{position}(P, \phi)}{(L - r)/2r}, \quad P = r, 3r, 5r, \dots, (L - r)/2r \quad (6)$$

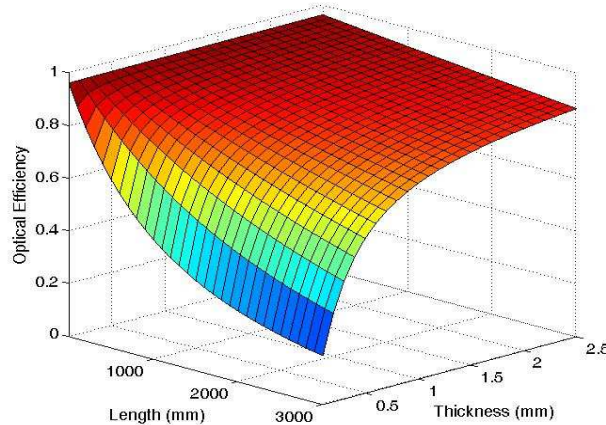


Fig. 4. The tradeoff between concentration and efficiency is governed by the equations in Section 2. Waveguide length and thickness vs. optical efficiency is plotted for F/3 lenses coupled at $\phi = 60^\circ$.

3. Waveguide coupling

3.1 Approach

Waveguide coupling requires localized features to be visible from within the slab to redirect incoming light into angles which exceed the critical angle for TIR. The simplest approach uses diffuse scattering surfaces on the waveguide in a manner similar to flat panel backlighting, but offers minimal control over exiting ray angles [14]. Alternatively, fluorescent dyes found in luminescent solar concentrators can absorb and re-emit light into potentially guided modes [15]. However, omnidirectional emission leads to similar coupling inefficiencies associated with diffuse scatter. Gratings and holograms have previously demonstrated waveguide coupling and offer precise angular control of the diffracted light [16,17]. The primary drawback associated with diffractive coupling is strong wavelength dependencies which hinder efficiency when used with broad spectrum illumination.

Specular reflections provide clearly defined reflection angles at all wavelengths. Reflections from TIR-based prisms or mirror-coated facets placed on the waveguide surface tilt the entire cone of focused sunlight into the waveguide. Similar surface texturing has been used in PV cell enhancement to extend photon lifetimes within active layers [18,19]. Marginal rays at the lens focus require the largest tilt to TIR at the core/cladding interface. Increasing the NA of the waveguide allows steeper ray angles to guide, however, these rays experience more decoupling and absorption losses due to increased optical path length. Assuming a planar fold mirror, the angle of the steepest marginal ray after reflection limits the lens $F/\#$ for a given waveguide NA.

3.2 Alignment

For efficient coupling, the lens array must be well-aligned to the patterned waveguide. Systems with few coupling features can be actively aligned by translating the lens array with respect to the waveguide. The couplers may be repositioned to collect off-axis illumination and extend the angular acceptance of the concentrator through micro-tracking movements. High concentration systems utilize very small coupling areas in conjunction with long guiding slabs. A 300x geometric concentrator requires $<20\mu\text{m}$ lateral alignment and $<0.01^\circ$ rotational accuracy about the slab center, normal to the plane of incidence. Precise, active alignment becomes exceedingly difficult for large-area optics.

Our alternative approach molds the coupling facets within a photosensitive polymer. An ultraviolet (UV) dosage through the lens array induces cross-linking at each focal plane. After exposure, the uncured polymer is removed while the couplers at image focus remain as part of the final device. The process is analogous to photolithography with the lens array acting as a mask. Since no alignment occurs between the lens focus and coupler, we refer to this process as self-aligned fabrication. The angular extent of the exposure source defines the coupler size and therefore the angular acceptance of the concentrator. Most importantly, the process fixes the coupling features at the lens focus and eliminates the need for alignment after fabrication. Self-alignment can be performed over large areas and remains compatible with roll manufacturing techniques. A more detailed description of the fabrication process is discussed in Section 5.

3.3 Design

Specifying self-alignment as a fabrication method imposes constraints on the coupler profile. The molding process requires a repeatable, faceted structure since features are not actively placed on the waveguide. 45° fold mirrors recurring in a triangular or sawtooth manner reflect normal incidence rays at 90° , which immediately strike the adjacent facet, and decouple upon second reflection. Conversely, 120° apex symmetric prisms have the unique ability to tilt normally incidence light to 60° with respect to the slab surface. This angle is exactly parallel to the adjacent facet and the ray completely avoids shadowing effects. Marginal rays

reflecting at shallower angles strike the adjacent facet at grazing incidence and continue to satisfy TIR. The prism configuration couples light equally in both directions resulting in output apertures located at opposite edges of the slab. Figure 5 shows the 120° symmetric prism and coupling functionality.

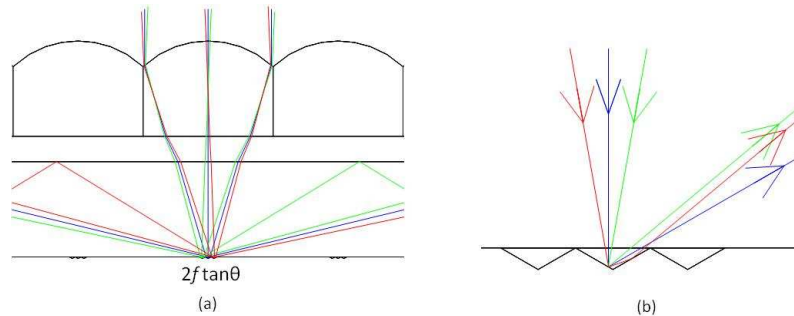


Fig. 5. The 120° symmetric prism reflects light at angles that TIR without shadowing from adjacent facets. The lens focal length and acceptance angle define the coupler size (a). A second reflection from the adjacent prism (red ray) matches the angle of the opposite marginal ray (green ray) and still exceeds the critical angle (b) for efficient guiding within the slab.

4. System optimization

We performed Monte Carlo ray tracing using ZEMAX EE non-sequential analysis software to model and optimize the efficiency of the micro-optic concentrator. The analysis assumed spherical, plano-convex refractive lenses forming a focus on the backside of a slab waveguide patterned with 120° coupling facets. Lens aberrations, Fresnel reflections, dispersion and material absorption were included in optical efficiency calculations. Simulations used weighted AM1.5 sunlight from 0.4 to 1.6μm at ± 0.26° field angles.

Our first design simulated a BK7 ($n_d = 1.5168$, $\alpha = 3 \times 10^{-6} \text{cm}^{-1}$) glass lens array and F2 glass waveguide ($n_d = 1.620$, $\alpha = 1.8 \times 10^{-4} \text{cm}^{-1}$) with a 200μm air cladding ($n_d = 1.0$) [20]. A single layer MgF₂ antireflection coating was placed on the first lens surface. The large index contrast enabled 2.38mm diameter, F/2.45 lenses to focus onto 78μm coupling regions attached to a 1mm thick waveguide. 90% optical efficiency occurred at 73x geometric concentration. At 300x, the system reached 81.9% optical efficiency. These values are comparable to Fresnel lens transmission efficiencies, however, this system has a 600mm aperture and is <10mm in total thickness [21].

Air claddings have practical concerns since the precision air gap must be maintained over large areas. Fluoropolymers such as LS-2233 (NuSil Technology, $n_d = 1.33$) are low-index coatings that can be applied directly to the waveguide surface as a cladding. To further reduce cost, the simulated glass array was replaced with a 500μm layer of cycloolefin polymer lenses (Zeon Corp, 480R, $n_d = 1.5253$) placed on a BK7 substrate. The final design used 2.79mm diameter, F/4.11 lenses focused onto 114μm coupling regions. 90% efficiency occurred at 49x geometric concentration and 78.5% efficiency at 300x. Larger F/# and coupling areas stemmed from the reduced waveguide NA and led to slightly more decoupling loss. Efficiency versus geometric concentration for both modeled systems is plotted in Fig. 6.

Spectral performance of the concentrator designs is shown in Fig. 7. Each provided excellent coupling and transmission over most of the solar spectrum with 84.8% and 81.4% peak efficiencies for air and LS-2233 claddings, respectively. The polymer lens array produced higher dispersion than BK7 lenses and accounted for coupling losses at lower wavelengths. Additionally, material absorption between 1.1 and 1.5μm occurred within the lens array and is typical of polymer optics [22]. Atmospheric water vapor absorbs large bands of the infrared spectrum, thereby negating much of the reduced performance at these wavelengths [23].

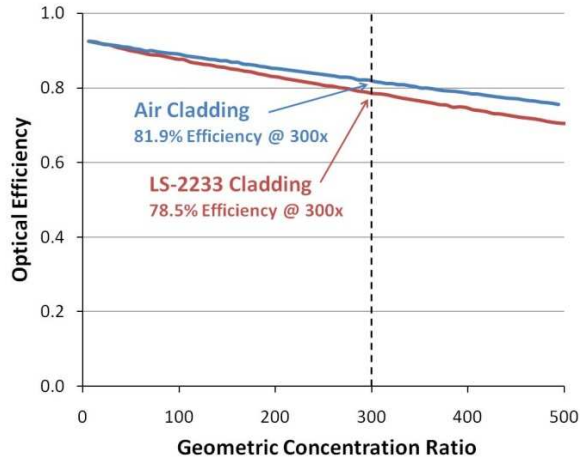


Fig. 6. Optical efficiencies for air (blue line) and LS-2233 fluoropolymer (red line) clad concentrator designs are plotted as functions of geometric concentration ratio. The LS-2233 design required larger coupling regions, but eliminated precision air gaps for simplified assembly.

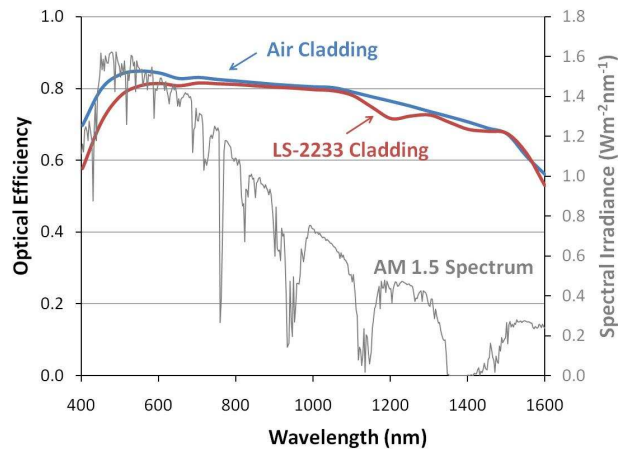


Fig. 7. Spectral performance for air clad (blue line) and LS-2233 fluoropolymer designs (red line) are plotted at 300x geometric concentration. The LS-2233 design also included a polymer lens array which increased dispersion and near infrared absorption. AM1.5 solar spectrum (grey line) is plotted on the right axis.

The angular acceptance of the concentrator depends on the coupler size compared to the demagnified image formed by the sun. When the coupling area matches the $\pm 0.26^\circ$ image height, exact alignment between the concentrator and sun's position is needed. Though very efficient, this configuration places strict requirements on mechanical tracking accuracy. Oversized coupling regions extend the acceptance angle by allowing the focus to remain incident on the coupler even when slightly misaligned to the sun. Larger coupling regions also increase the likelihood of waveguide decoupling which reduces optical efficiency. Figure 8 plots the normalized optical efficiency versus acceptance for the 300x, F/2.45 air clad concentrator. $78\mu\text{m}$ diameter coupling regions accept only the $\pm 0.26^\circ$ angular spread of the sun. Increasing the coupling diameter to $156\mu\text{m}$ provides $\pm 0.63^\circ$, albeit with 22% less efficiency. Acceptance angle is an additional parameter which can be optimized based on the desired system performance. Angular extent of the UV illumination used during self-aligned fabrication controls the coupler size and is discussed in following section.

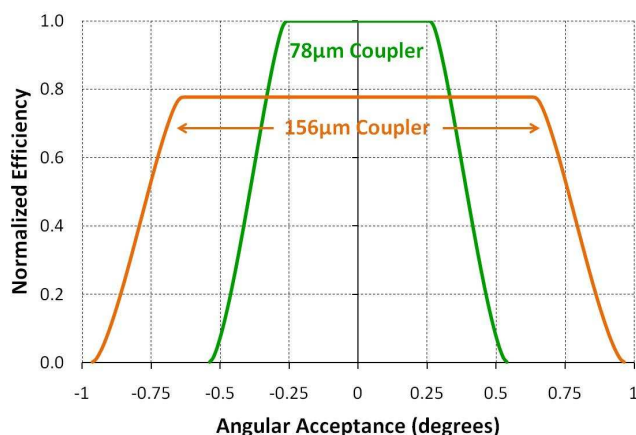


Fig. 8. The size of the coupling region determines the angular acceptance of the concentrator. 78 μm diameter couplers (green line) capture only the $\pm 0.26^\circ$ extent of the sun. Larger coupling regions (orange line) increase acceptance angles, but also increase decoupling losses.

5. Concentrator prototype

The simulated concentrators in Section 4 utilized lens profiles optimized for light coupling into supported waveguide modes. However, to demonstrate the viability of self-aligned fabrication and coupling, we constructed a prototype concentrator from an off-the-shelf lens array which did not contain the ideal refractive contour. We began with a commercially available 2.3mm diameter F/1.1 hexagonal lens array. The very low F/# optic suffered from strong spherical aberration and produced steep marginal rays which could only be guided with air claddings. We chose a 75mm long by 1mm thick BK7 glass slab waveguide which yielded 37.5x geometric concentration with symmetric coupling. 50 μm pitch, 120° prisms embossed on a flexible substrate were molded using SU-8 photoresist. SU-8 is an epoxy-based negative photopolymer well-suited for micro-optic replication and sunlight coupling because of its optical clarity, good chemical resistance and operating temperatures above 200°C [24].

5.1 Self-aligned fabrication

Self-aligned fabrication began by spin-coating SU-8 photoresist on one side of the glass slab. SU-8 is formulated with gamma butyrolactone which was fully removed by extending the soft-bake timing by 20%. Heating the resist above the glass transition temperature (50°C) maintained a pliable state which could be molded [25]. The flexible prism array master was pressed into the hot resist and baked under weight and vacuum to remove any trapped air. <0.5% polymer shrinkage and no impact on UV cross-linking have been observed with this vacuum molding procedure [26].

After baking, the prism master was peeled away from the slab and the lens array was placed on the top surface, leaving a 45 μm air gap cladding. 300 mJ/cm² of UV illumination through the lens array cross-linked the photoresist at each lens focus. Beam divergence controlled the coupler size and ultimately the angular acceptance of the concentrator. We constructed an exposure source using a mercury-arc lamp imaged through an adjustable iris, and collimated by a parabolic mirror. Adjusting the diameter of the iris altered the divergence of the UV illumination. Prior to development, we deposited an aluminum coating over the entire molded surface to create reflective coupling facets. Un-exposed resist was removed through immersion in PGMEA developer in conjunction with heat and ultrasonics. A more detailed description of the fabrication process is found in Ref [27].

5.2 Experimental measurement

The F/1.1 lens array created 200 μm spots on the backside of the waveguide when fabricated with $\pm 0.26^\circ$ light. Lens aberrations and the image intensity profile gave rise to a 50 μm annulus of partially-cured photoresist surrounding each coupler. These faceted regions are relatively large and increase waveguide decoupling loss, however, self-aligned fabrication consistently yielded accurate, localized prism molding, as seen in Fig. 9.

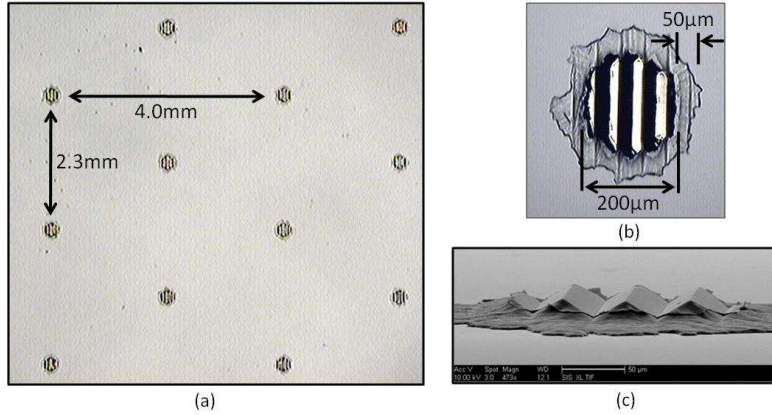


Fig. 9. 120° coupling facets appearing at each lens focus (a) are fabricated using self-alignment. Lenses form 200 μm images with 50 μm irregular annuluses which contribute to loss (b). An SEM image (c) captures the coupler profile.

The lens array is mounted on a translation stage to demonstrate the effect of misalignment. With the lens focus aligned to the coupler, the output edge of the concentrator appears bright and very uniform in intensity, as seen in Fig. 10(a)-left. When translated by 195 μm , <10% of the incident light couples into the waveguide, Fig. 10(a)-right. A false color image of the aligned system, Fig. 10(b), shows the homogenous flux output. Intensity roll-off appears at the extreme edges of the aperture and is associated with the narrow width of the prototype.

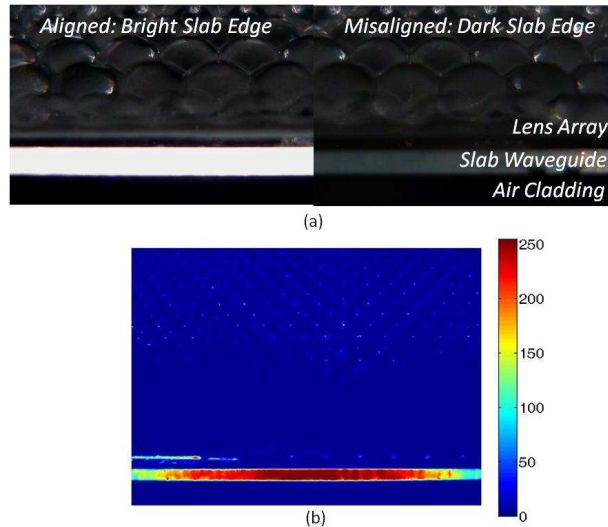


Fig. 10. When the system is aligned (a, left), light couples into the waveguide and exits the slab edge. Misalignment between the lens array and facets lets light pass directly through the system (a, right) with almost no waveguide coupling. A false color image of the output (b) reveals flux uniformity.

The steep curvature of the available lens array contained small gaps between array sub-apertures without optical power. The consequence was only 72.5% fill-factor, with the remaining regions contributing to loss. Monte Carlo ray tracing of the prototype concentrator calculated 44.8% optical efficiency at 37.5x when considering all loss sources. The efficiency was experimentally measured using a calibrated photodetector and integrating over the area illuminated by white light, collimated to $\pm 0.26^\circ$. We measured 32.43% of the input light exiting along both slab edges. Slight coupler variations and diffuse slab edges accounted for difference between the simulated and measured systems. Figure 11 plots the optical efficiencies of the simulated and experimental systems.

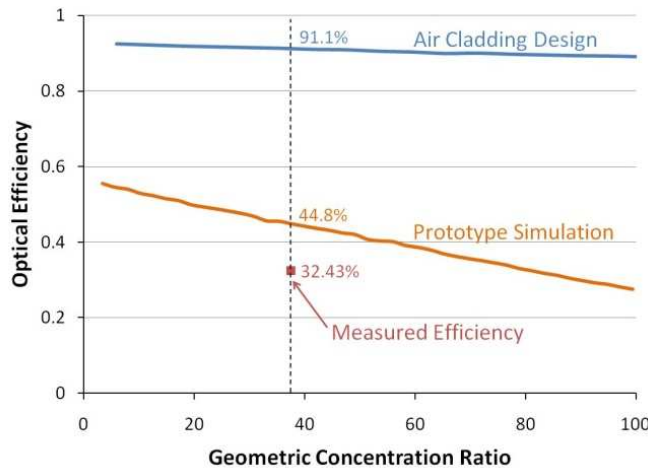


Fig. 11. A 37.5x prototype concentrator constructed from off-the-shelf components demonstrated the self-aligned fabrication process, but was inefficient compared to optimized designs. Lens fill-factor and aberrations caused the majority of the observed loss.

We transported the system outdoors to test coupling with actual sunlight. Figure 12 shows the system outside with a bright output edge when collecting direct sunlight. The short focal length of the F/1.1 lenses created only small changes in image position when misaligned to the sun. The prototype system reached 90% of its maximum optical efficiency with $\pm 1^\circ$ angular acceptance.

The main goals of the prototype concentrator were to demonstrate self-aligned fabrication and light coupling from multiple sub-apertures into a common waveguide. The optical efficiency of the prototype system was significantly lower than the optimized simulations using custom optical elements. Despite its relative inefficiency, our experimental measurements were in close agreement with our optical model and support the notion that optimized designs would also perform with high efficiency.

We are currently pursuing variations of the basic structure described here to increase both concentration and optical efficiency. Reflectors covering one of the symmetric outputs can redirect all sunlight to a single PV cell. Modifications to the coupler orientation may enable concentration in the orthogonal direction in addition to confinement within the slab thickness. Also, secondary concentrators placed at the output apertures can aid in light extraction and coupling into PV cells. These future additions remain compatible with roll processes and further advance the low cost and efficiency of the micro-optic slab concentrator.

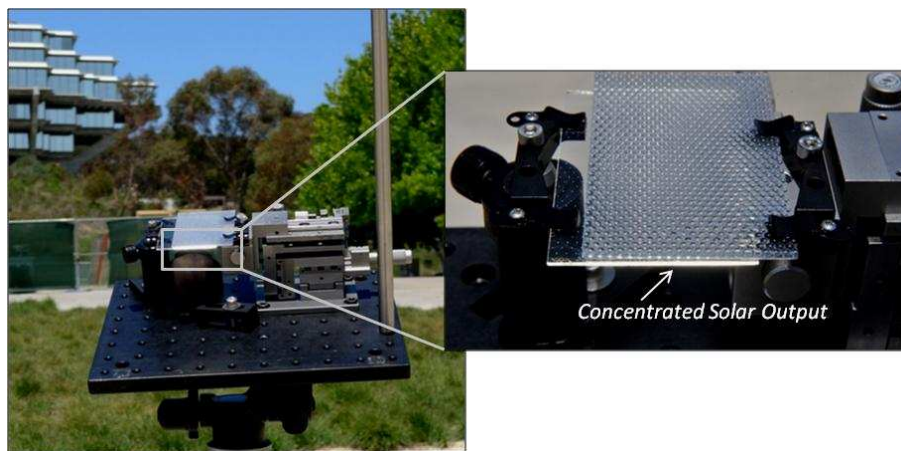


Fig. 12. A prototype concentrator was used to collect sunlight in an outdoor setting. Inset: When properly aligned to the sun, light incident on the lens array surface couples into the waveguide and exits at the waveguide edge, appearing as a bright line.

6. Conclusion

CPV relies upon inexpensive concentrator optics and assembly to offset the high cost of very efficient solar cells. We demonstrate how a multimode slab waveguide can be used as secondary optic to collect and homogenize sunlight focused by a two-dimensional lens array. Reflective facets fabricated on the backside of the waveguide act as fold mirrors to couple sunlight into the waveguide at angles which exceed the critical angle for TIR. These facets occupy a small fraction of the total waveguide surface and enable high geometric concentrations despite decoupling loss if light strikes a subsequent coupling region.

The performance of the concentrator depends on several key design points such as the lens $F/\#$, waveguide NA and tilt angle of the coupling facets. We selected a 120° symmetric prism array to reflect normally incident light at 60° without any shadowing loss from adjacent prisms. Optimized 300x designs reached 81.9% optical efficiency using all glass components, and 78.5% efficiency when switching to a polymer lens arrays and fluoropolymer cladding.

Waveguide coupling facets are created by first molding the structure within a photopolymer and using the lens array image plane as a mask during cross-linking. The self-aligned fabrication technique ensures proper alignment between thousands of individual coupling points and remains compatible with high-volume, roll processing. We demonstrated self-aligned fabrication using off-the-shelf components to create a 37.5x prototype concentrator with 32.4% optical efficiency. Systems with $>80\%$ are expected when using a custom lens array with 100% fill factor and minimal aberration. CPV with multimode waveguides opens a new design space for large-scale concentrator optics with the added benefits of flux uniformity and fewer PV cells in a thin, planar geometry.

The authors would like to thank Wavefront Technology, Inc. for providing components used during fabrication. We would also like to acknowledge the National Science Foundation (NSF) for support under the Small Grants for Exploratory Research (SGER) and the California Energy Commission (CEC) for support under the Energy Innovations Small Grant (EISG) program.